Nuclear Magnetic Resonance and Molecular Modeling Study on Mycophenolic Acid: Implications for Binding to Inosine Monophosphate Dehydrogenase

Gergely M. Makara,† György M. Keserû,§ Mária Kajtár-Peredy,‡ and Wayne K. Anderson*,†

Department of Medicinal Chemistry, School of Pharmacy, State University of New York at Buffalo, Buffalo, New York 14260, Department of Chemical Information Technologies, Technical University of Budapest, St. Gellért tér 4, Budapest H-1111, Hungary, and Central Research Institute for Chemistry, Hungarian Academy of Sciences, POB 17, Budapest H-1521, Hungary

Received August 11, 1995⊗

The conformation of the sodium salt of mycophenolic acid (MPA), a potent inhibitor of inosine monophosphate dehydrogenase (IMPD), derived from 1D DIFNOE and 2D ROESY experiments in water and molecular dynamics (MD) is described. The hexenoic acid side chain conformation consistent with the NMR data was similar to that seen in the X-ray structure of MPA. The solution conformation was applied in a molecular modeling study in order to explore the potential features of enzyme binding. Our results, based on striking similarities in molecular volume and electrostatic isopotential between MPA and cofactor NAD^+, lead to the suggestion that MPA is capable of binding to the nicotinamide site of IMPD and mimicking the NAD^+ inverse regulation of the enzyme. In addition, our proposed model is in good agreement with the observed high affinity of the dinucleotide analogues thiazole- and selenazole-4-carboxamide adenine dinucleotide to IMPD.

Introduction

Mycophenolic acid (MPA, **1**) was first reported in the last century, and since that time, this mold metabolite has assumed a role of central importance as an inhibitor of inosine monophosphate dehydrogenase (IMPD). A prodrug of MPA, the morpholinoethyl ester, is currently in advanced clinical trial as an immunosuppressant, and MPA has been shown to possess significant antineoplastic,[1] antiparasitic,[2] and antiviral activity. It is also very active against psoriasis.[4] Other IMPD inhibitors are also known, and for convenience, we have classified them into three categories based upon the mode of enzyme binding:[5] type I inhibitors are inosine 5′-monophosphate (IMP)/xanthosine 5′-monophosphate (XMP) analogues, type II inhibitors are NAD^+/NADH analogues, and type III inhibitors are multisubstrate inhibitors. MPA is a type II inhibitor that requires no metabolic activation[6] and, as such, can be compared with other type II inhibitors such as tiazofurin and selenazofurin. Tiazofurin and selenazofurin must first be converted to the adenine dinucleotides "TAD" (thiazole-4-carboxamide adenine dinucleotide, **3**) and "SAD" (selenazole-4-carboxamide adenine dinucleotide, **4**) in vivo. Enzyme kinetic studies have demonstrated[5a,6] that MPA, TAD, and SAD are noncompetitive inhibitors of IMPD with respect to NAD^+. In the case of an ordered sequential mechanism, this means that they bind at the cofactor site in the presence and absence of the substrate. The mycophenolic acid- and tiazofurin-binding site has been further localized to the nicotinamide end of the dinucleotide binding region.[6] However, no X-ray structure of IMPD has been solved, so the specific steric requirements of cofactor and inhibitor binding are not known. Structural features of TAD and SAD binding to other dehydrogenases have been investigated,[7] but no model for binding of mycophenolic acid has been reported. The question arises, can mycophenolic acid mimic NAD^+ in its binding to IMPD?

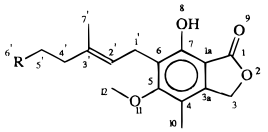

1 R=COOH
2 R=COO^-

Figure 1.

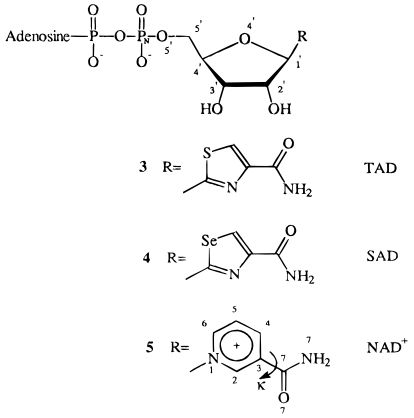

Figure 2.

In this study, we present an analysis of the conformation of the ionized MPA (**2**), the form likely to dominate at physiological conditions in aqueous solution. We report the results of molecular dynamics and restrained simulated annealing calculations applying distance data obtained from 1D NOE experiments.

Nuclear Magnetic Resonance. Solution conformational properties of **2** were examined by NMR methods in D_2O solution. ^{1}H-NMR signals of **2** were assigned, and the chemical shifts are given in Table 1. Allylic C(7′)H, and benzylic C(1′)H_2 signals were found to be broader than expected which was explained by long range allylic and homoallylic couplings. Methylene protons of the C(1′)H_2 group were isochronous and exhibited an averaged vicinal coupling constant. The

† State University of New York at Buffalo.
‡ Hungarian Academy of Sciences.
§ Technical University of Budapest.
⊗ Abstract published in *Advance ACS Abstracts,* February 1, 1996.

0022-2623/96/1839-1236$12.00/0

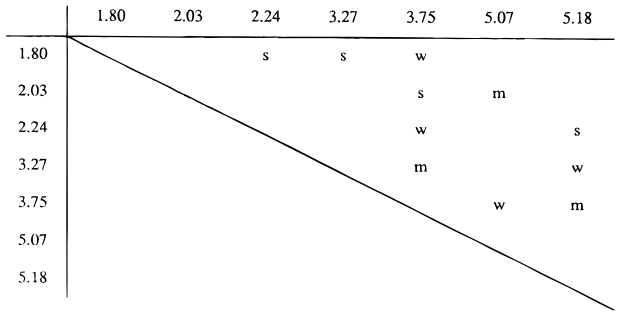

Figure 3. Qualitative 2D ROESY matrix for **2** (s, strong; m, medium; w, weak).

Table 1. Assignment of the 400 MHz Proton NMR Signals for **2**

proton	chemical shift (ppm)	multiplicity	coupling constant (Hz)
$C(7')H_3$	1.80	s	
$C(10)H_3$	2.03	s	
$C(4')H_2C(5')H_2$	2.24	m	
$C(1')H_2$	3.27	d	6.2
$C(12)H_3$	3.75	s	
$C(3)H_2$	5.07	brs	
C(2′)H	5.18	t	6.2

Table 2. 1D NOE Intensities and Calculated Proton−Proton Distances for **2**

irradiated at	enhancement at	intensity (%)	distance (Å)
$C(12)H_3$	$C(7')H_3$	0.46	5.67
	$C(10)H_3$	1.31	1.99
	$C(4')H_2C(5')H_2$	0.09	
	$C(1')H_2$	0.69	3.78
	$C(3)H_2$	0.12	
	C(2′)H	0.92	2.83
$C(10)H_3$	$C(3)H_2$	0.75	3.48
	C(2′)H	0.22	
$C(7')H_3$	$C(4')H_2C(5')H_2$	1.07	2.44
	$C(1')H_2$	1.07	2.44

$C(4')H_2C(5')H_2$ group gave rise to an unresolved multiplet because of the nearly identical deshielding effects of the carboxylate group and the double bond, respectively. Line broadening caused by the above-mentioned effects led us to study only the mutual steric disposition of protons producing singlet signals. The preferred conformation adopted by **2** in aqueous solution has been determined by steady state 1D NOE and 2D ROESY measurements. 1D DIFNOE irradiations and enhancements are listed in Table 2. 1D nuclear Overhauser effects were supported by 2D results which are shown in Figure 3. The DIFNOE spectra were used to calculate interatomic proton−proton distances, using the two-spin approximation. Due to the close chemical shifts and the pseudoequivalent nature of geminal methylene protons as well as the lack of aromatic ortho protons, distances were calibrated using the time-averaged distance (3.48 Å) between the protons of the almost fixed $C(10)H_3$ and $C(3)H_2$ groups. The calculated distances are given in Table 2.

Molecular Dynamics Simulations. The free molecular dynamics and the restrained simulated annealing calculations were carried out[8] in vacuo at high temperature in order to explore the entire potential surface. First, unrestrained MD was completed for 100 ps at 700 K starting from the energy-minimized X-ray structure (PM3 following deletion of acidic hydrogen) to provide an insight into the conformational behavior of the molecule. Analysis of the snapshots with the Family option of SYBYL resulted in 16 conformational families providing 21 representatives (the highly populated families delegated more than one representative). All conformations were optimized by molecular mechanics followed by semiempirical PM3 calculation. The relevant intramolecular distances were compared to the experimental data. Centroid coordinates of the chemically equivalent protons were determined and used in calculation of restraints.

The restrained MD calculation was carried out in vacuo by SYBYL's simulated annealing module over 10 cycles with an exponential annealing function starting from the same optimized crystal structure as above. A total of four experimental distances with force constants of 15 kcal/mol Å^2 were used to constrain the freedom of motion. These were characteristic for the behavior of the solute molecule and associated with singlet protons on the NMR. The starting temperatures were set to 700 K for 2 ps simulation time; then the systems were allowed to cool to 200 K over 5 ps, and the final conformations were optimized with molecular mechanics using the same restrain values as in the MD. The 10 resultant structures were energy minimized with PM3 (precise criteria) giving rise to three distinct conformations that were subject to evaluation.

An additional simulated annealing calculation was carried out in water, starting from the same structure, to confirm the results of the simulations run in vacuo. The constrained solute was surrounded by 750 water molecules in a lattice and equilibrated for 2 ps at 300 K. Then the temperature was set to 700 K for 1 ps and lowered stepwise to 200 K over 2.25 ps. The conformational behavior of **2** was examined over the last 1 ps.

Conformational Analysis of NAD^+ and MPA. Our preliminary investigation of molecular similarities between the X-ray structures of MPA and NAD^+ extracted from the crystal structure of human alcohol dehydrogenase (an A-type enzyme) suggested that the lactone carbonyl, the carboxylate, and the aromatic moiety of MPA could be superimposed on the carboxamide, phosphate, and pyridine groups of NAD^+, respectively. The fit resulted in comparable molecular volumes and electrostatic characters using a flexible fitting procedure;[9] however, the amide in the cofactor adopted the more stable cis conformation[10] ($\kappa = 0°$). No such fit was found with the trans ($\kappa = 180°$) stereoisomer of NAD^+.

In order to examine the naturally occurring cofactor conformations, the crystal structures of all $NAD(H)^+$-bound dehydrogenases were downloaded from the Brookhaven Protein Data Bank[11] and the cofactors were extracted and analyzed. In the A-type dehydrogenases (*i.e.*, the ribose−nicotinamide glycosyl bond is anti with the carboxamide projected away from the ribose), $NAD(H)^+$ adopts a more extended conformation than in the B-type. The B-type enzymes bind $NAD(H)^+$ in a syn orientation with an intramolecular interaction of the phosphate oxygens with the amide moiety.[12] IMPDs are B-type dehydrogenases,[13] however, TAD and SAD has been shown to favor the anti conformation of the glycosyl bond.[14] The opened (anti) conformation of $NAD(H)^+$ gives rise to considerably better fit with MPA; thus the coordinates of NADH derived from glutathione reductase[15] were selected for further study being the only deposited enzyme with bound cis-anti stereoisomer

Table 3. Intramolecular Distances (Å) of Relevant Protons[c] for Various Conformations of **2**

	ϕ (deg)	H_f (kcal/mol)[a]	C(12)H_3−C(7′)H_3	C(12)H_3−C(1′)H_2	C(12)H_3−C(2′)H	C(7′)H_3−C(1′)H_2	C(12)H_3−C(4′)H_2C(5′)H_2
exp			5.67	3.78	2.83	2.44	<6.0[b]
2a (X-ray)	−120.8		6.72	3.94	3.30	3.35	4.81, 6.58
2b	−132.3	−270.6	6.50	3.77	3.52	3.13	6.25, 7.37
2c	−177.1	−263.1	5.60	4.04	3.29	3.05	5.00, 5.45
2d	−158.7	−261.3	6.01	4.16	2.75	3.01	5.39, 4.25
2e	152.3	−261.6	4.78	4.25	3.47	3.03	3.09, 4.76
2d:**2e** = 3.1			5.71	4.18	2.93	3.01	4.81, 4.37

[a] Calculated by PM3. [b] From qualitative 2D ROESY. [c] Chemically equivalent.

of the cofactor. Two dihedral angles (O4′−C1′−N1−C6 [χ] and C2−C3−C7−O7 [κ] were designed at rotatable bonds and gradually modified (10° increment) because these parameters have yet been shown[16] to possess widely diverse values depending on steric requirements imposed by the enzyme active site. The rest of the molecule was left unaltered. All structures resulting from this operation were subjected to comparison with the selected model of mycophenolic acid (**2d**).

Electrostatic isopotential surfaces were computed for the selected superimposed pair at 1.1 × vdW radii from the Mulliken populations derived from semiempirical PM3 calculations with the point-charge method.[17] (Use of MOPAC charges produced an identical density surface for NAD^+ but a more negative one for MPA resulting in larger distinctions at the hydrophobic areas.) NAD^+ was modeled with the adenosine moiety replaced by a methyl group and optimized only for bond distances to release unfavorable strains without altering the conformation. The dot surfaces were displayed at 1.1 × vdW radii and colored by a fixed, identical scale of electrostatic isopotential for each molecule.

Results

Conformation of Mycophenolic Acid Sodium Salt. The MPA hexanoic acid chain has restricted conformational mobility due to the *E*-geometry of the 2′,3′-double bond and steric interactions with the two ortho substituents (C5 and C7) on the rigid phthalide ring system. The C5 methoxy group is forced out of the plane of the aromatic ring because of the interactions with the C4 methyl group and the hexenoic acid side chain at C6. The restricted conformational mobility of the side chain is largely confined to the region between C6 and C4′. The C5′−C6′ carboxylate terminus can rotate more freely (barrier *ca*. 1 kcal/mol) and adopt a number of different conformations (a particularly important feature because the corresponding anionic phosphate in NAD^+ possesses similar flexibility). The NOE experiments provided the key interatomic distances in the region between C6 and C4′.

Investigation of the representatives derived from the free MD simulation revealed that in the most stable conformation (**2b**; Figure 4), the carboxylate and the phenol hydroxyl form an intramolecular hydrogen bond most likely representing the global energy minimum. However, the existence of such a macrocyclic intramolecular interaction is highly questionable especially in polar solvents. Table 3 shows that the measured distances in this conformation are indeed not in correspondence with the NMR data. Among the pool of representatives, one conformation (**2c**) was found to comply with the experimental distances within reasonable margin of errors (Table 3). Interestingly, **2c** is strikingly similar to the X-ray structure of mycophenolic acid, the only distinction being C6−C1′−C2′−C3′ torsion angle −177.1° instead of −120.8°. Seven of the 10 structures provided by the restricted simulated annealing calculation were found to be identical with **2c** (ignoring the flexible C5′−C6′ terminus). Two cycles gave rise to the global minimum **2b**, and one cycle resulted in a conformation that is of unique character because the methoxy group was facing away from the C6 hexenoic acid side chain; therefore, the distances between the methoxy and the C1′, C2′, and C7′ protons were significantly larger than those calculated from NOE enhancements (data not shown). The side chain also adopted the conformation of **2c** over the investigated period of time of the MD calculation in water.

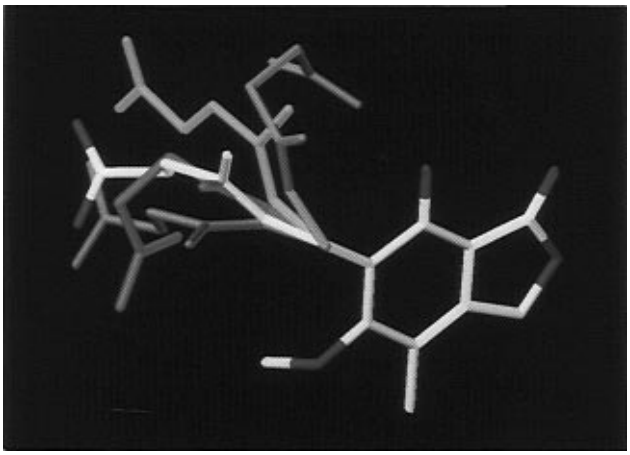

Figure 4. Conformations of **2**: cyan, **2a** (from X-ray); orange, **2b**; purple, **2c**; colored by atom types (C = white, O = red), **2d**; green, **2e**.

Comparison of interatomic distances within the X-ray and the computer-generated structures to those measured by NOE experiments shown in Table 3 reveals that good agreement is achieved in the case of **2c**. This conformation constituted one of the families in free MD and dominated among the final snapshofts of the simulated annealing cycles. The greatest violation, 0.6 Å, occurs for the C1′−C7′ protons, but it should be emphasized that **2c** comprises the least attainable distance between these atoms; thus this deviation appears to derive from experimental error. Although our findings are confirmed by both dynamics simulations, it is unlikely that such a small molecule with some restricted but yet rotatable bonds as mycophenolic acid would exclusively adopt one definite conformation in solution. The behavior of the molecule could rather be characterized by an interval of the variable(s); therefore, the C6−C1′−C2′−C3′ torsion angle [ϕ] was designated as rotatable bond starting from **2c**, and the appropriate distances were continuously monitored to show that the NOE requirements can be fulfilled with acceptable deviation between the boundaries of −159° and 152°,

Table 4. rms Values for Least-Squares Fit of **2d** and NAD^+ as a Function of the Altered Dihedral Angles of NAD^+ Derived from Glutathone Reductase

no. of atom pairs	$\chi = 7.6°$, $\kappa = 10.8°$ (X-ray str)	$\chi = 0°$, $\kappa = -30°$	$\chi = -8.9°$, $\kappa = -30°$	$\chi = -30°$, $\kappa = 0°$
5[a]	0.580	0.382	0.398	0.585
15[b]	0.814	0.712	0.648	0.630

[a] Fitting points are O7(NAD^+)−O9(MPA), C7−C1, C3−C8, N1−C6, and P_N−C6′ atom pairs. [b] Fitting points are O7(NAD^+)−O9(MPA), C7−C1, C3−C8, N1−C6, P_N−C6′, C5−C4, N7−O2, C4−C3a, C6−C5, C2−C7, C1′−C1′, O4′−C2′, C4′−C3′, C5′−C4′, O5′−C5′ atom pairs.

values associated with local energy minima (PM3) **2d**,**e**, respectively. It should be pointed out that **2d** corresponds to the conformation attainable by PM3 starting from X-ray structure, within these angles the heat of formations only slightly differ, and in addition, their 3:1 ratio gives rise to better correlation with the experimental data than any of **2a**−**e** in itself (Table 3). Thus, it seems likely that the motion of the side chain of mycophenolic acid in aqueous solution is confined to a particular region that could be best described by **2d,e** as boundary conformations.

Conformational Analysis of MPA and NAD^+. Manual fitting or computer-aided construction of receptor models can be used to probe the potential binding features of ligands to an uncharacterized receptor. The latter requires several active inhibitors to be included in order to increase the correlation between calculated energy and bioactivity.[18] An appropriate number of inhibitors is not available for IMPD because TAD and SAD belong to natural nucleoside analogues of NAD^+. Thus mycophenolic acid is the only compound that possesses a possible unique configuration among inhibitors that are assumed to bind to the nicotinamide-binding site. We have found several structural features in MPA that could provide the base of comparison of NAD^+. The lactone carbonyl, carboxylate, and the aromatic moiety of MPA can serve as possible natural replacements of the carboxamide, phosphate, and pyridine groups of NAD^+, respectively. Moreover, the meta substitution pattern of the nicotinamide could be easily identified in the bicyclic lactone ring.

Hydrogen bonding plays a very important role in binding to dehydrogenases; therefore, we designated the potential hydrogen-bonding participants, the C6′ carboxylate and the C1 carbonyl, of MPA as the most significant contributors to the binding energy. These groups were oriented as closely as possible to the P_N phosphate and C7 amide of NAD^+; hence O7(NAD^+)−O9(MPA), C7−C1, C3−C1a, N1−C6, and P_N−C6′ were selected as pairs in the least-squares fit calculations. In a separate fit analysis, all nonhydrogenoid atoms of MPA were paired with the closest nonhydrogenoid atom of NAD^+ (Figure 5) except for C3, C10, C7′, and the methoxy group. Fit of conformations **2d** and NAD^+ derived from glutathione reductase resulted in rms values[19] of 0.580 and 0.814; however, gradual modification of χ and κ torsional angles from 7.6° and 10.8° to −8.9° and −30° significantly improved these values and, generally, resulted in similarly reasonable results within the interval of $\chi = 0°$, $\kappa = -30°$, and $\chi = -30°$, $\kappa = 0°$ (Table 4). It also should be pointed out that flexible fit that allows small alterations in both molecules produced even much lower rms values (data not shown). The

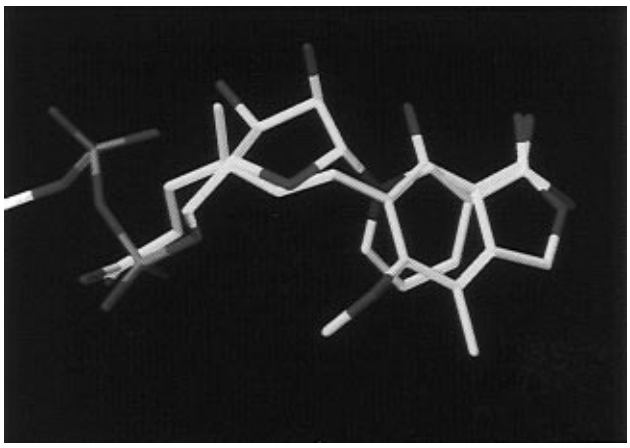

Figure 5. Superposition of **2d** and NAD^+.

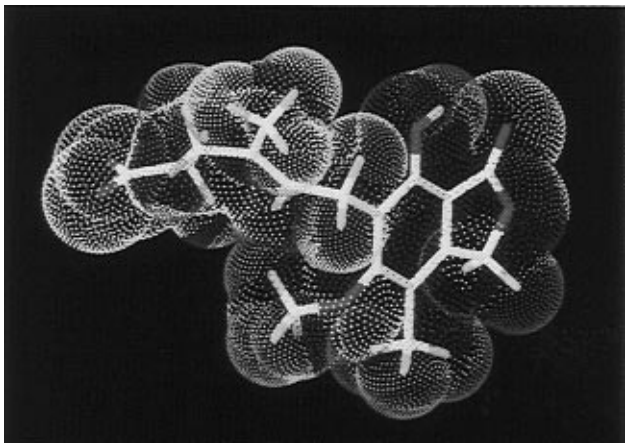

Figure 6. Electrostatic isopotential of **2d** on dot surface of 1.1 x vdW radii.

representation of the overlaid conformations on Figure 5 shows that this arrangement of the two molecules could also rationalize the role of the phenolic hydroxyl of MPA which is placed close enough to the C2′-OH of the ribose (O−O distance: 2.95 Å) and/or the positively charged N1 (N−O distance: 2.29 Å) to hydrogen bond with a suitably positioned residue in the active site which originally stabilizes NAD^+ through H-bonding or electrostatic interaction. However, this interaction requires the disturbance of the intramolecular H-bonding of the phenol with the lactone carbonyl to take place as we have previously proposed.[20]

Ligands that bind to the same active site of a particular enzyme are expected to possess comparable electrostatic properties which enable them to comply with the necessity of electrostatic complementarity with the enzyme-binding site. Accordingly, we examined the molecular electrostatic potentials (MEP) generated by **2d** and NAD^+ at 1.1 x vdW radii visualized by potential color method on dot surfaces (Figures 6 and 7). The overall charge is −1 in both cases. The MEPs were found very similar for the two distinct molecules. There are two strongly negative regions (<−25 kcal/mol) around the lactone carbonyl and the C5′−C6′ acetate and two very positive hydrophobic areas (>10 kcal/mol) between C1′−C7′ and C3−C10 carbons of **2d** that could be discovered at the same locations in NAD^+, while the pyridine ring seems to generate somewhat more positive EP above the plane than the bicyclic lactone. The only significant difference is the negative lactone O2 that has

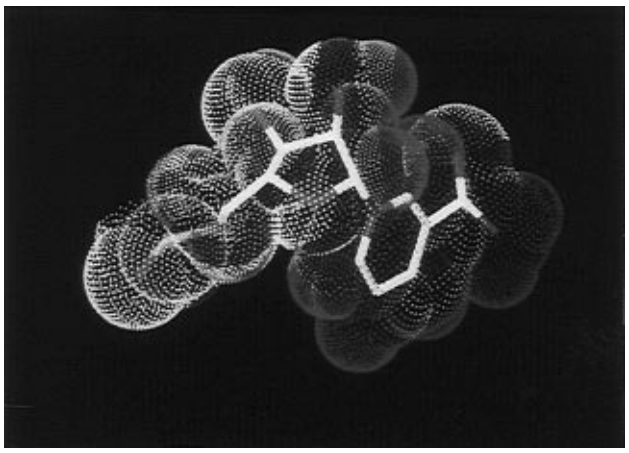

Figure 7. Electrostatic isopotential of NAD^+ on dot surface of 1.1 x vdW radii.

an opposite character than the positive $N(7)H_2$ in NAD^+, suggesting a distinct hydrogen-bonding feature of these moieties.

Discussion

The observation of same intramolecular contacts in different environments indicates the presence of intramolecular forces stabilizing a particular conformation of MPA. Both 1D and 2D NMR experiments supported the conclusion that, in an aqueous medium, the C5 methoxy group of MPA-Na is projected toward the C6 side chain in order to maximize hydrophobic van der Waals interactions and to minimize exposure to hydrophilic water. The methoxy protons are closer to the C2′ hydrogen than to protons of C7′ and/or C1′, as was found in the solid state. This arrangement is likely to be triggered by a chain of complex steric interactions of the substituents as follows. The C4 methyl group destabilizes the ring-opened hydroxy acid form of the phthalide lactone[21] due to a steric effect between C10 and C3 and induces the out-of-plane rotation of the methoxy along with the C6 side chain. The latter is a mutual effect providing significant steric bulkiness along with the same influence exerted by C7-OH which hinders any significant motion of the side chain already having its own rigidity (double bond). However, the C7′ methyl is also necessary to increase the rotational barrier and confine the hexenoic acid side chain to a narrow region. Thus the conformational freedom of mycophenolic acid seems to be restricted, a factor which may play an important role with respect to the high inhibitory potency of the compound toward IMPD.[22] It may be argued, therefore, that the bioactive conformation is similar if not identical with the solution conformation. Every structural modification that disrupts this conformation is expected to produce analogues with markedly decreased potency.

IMPDs belong to the family of B-type dehydrogenases[13] which have been shown to incorporate the $NAD(H)^+$ cofactor having a *syn*-glycosyl bond.[12] However, the potent inhibitors TAD and SAD have been shown to adopt an anti orientation ($-30° < \chi < 30°$) due to intramolecular electrostatic interaction between the ribose oxygen and the partially positively charged S/Se atoms.[14] This conformation has been found to be retained in enzyme-bound form, as well.[7] The K_i of TAD against IMPD is 2 orders of magnitude less than that for other dehydrogenases, and this can be attributed to the enthalpic and entropic penalty associated with the loss of this favorable intramolecular contact. This notion is further supported by the inactivity of oxazofurin (S/Se is replaced by an oxygen), an analogue that lacks the S/Se−ribose oxygen stabilization.[23] Our modeling study suggests that MPA could bind to a nicotinamide site if the adopted glycosyl bond is between 0° and 30°, which is in accord with the preferred TAD/SAD binding mode.

The ordered sequential mechanism exhibited by inosine monophosphate dehydrogenases requires that the substrate binds first before NAD^+ and, following the enzymatic reaction, NADH is released before the product. However, the enzyme−XMP complex can bind NAD^+ to form a ternary complex, resulting in an inverse regulation[6,24] of IMPD by NAD^+. The regulatory role of the cofactor on IMPD is, therefore, diminished in hypoxic tumor cells where NAD^+ levels are lower than normal.[25] Moreover, it also has been proposed, based on multiple-inhibitor experiments, that the inverse regulation does not simply occur by combining with the E−XMP but NAD^+, TAD, and MPA inhibit an additional enzyme form. Therefore, the mechanism must include an isomerization step.[6] In light of our findings, it seems possible that the nicotinamide binding site is involved in this conformational change to give rise to an altered active site environment. TAD- and MPA-like (anti) stereochemistry may result in an enhanced complementarity to the active site residues of IMPD in the course of inverse regulation mechanism, while the syn orientation is likely to be favored during the hydride transfer.

The selection of the adopted κ and χ values in $NAD(H)^+$ are frequently governed by the positions of the interacting amino acid residues rather than the exclusion of one isomer due to steric reasons.[7,26] In TAD and SAD, intramolecular hydrogen bond stabilizes (by *ca.* 9 kcal/mol) the trans ($\kappa = 180°$) carboxamide isomer;[16] therefore, superposition of TAD and **2d** places the amide N in close proximity with the carbonyl O9 of MPA. These two atoms are likely to participate in opposite type of H-bonding; thus the interacting active site residue must be such that is capable of being either donor or acceptor (*e.g.*, serine), or they could establish contact with different amino acids. This dilemma could be further explored by conformationally constrained TAD analogues and appropriately altered mycophenolic acid derivatives, which is part of an ongoing project in our laboratory.

Conclusion

In this study we propose, for the first time, a model of the bioactive conformation of mycophenolic acid bound to the nicotinamide site of inosine monophosphate dehydrogenase. The proposal is based on the conformation of the sodium salt of MPA obtained by analysis using NMR and molecular dynamics methods. The similarity of this conformation with that of MPA in the solid phase[27] suggests that the side chain is conformationally restricted, thus explaining the sensitivity of MPA toward structural modifications. This model was found to be in accord with the favored binding mode of other active inhibitors, TAD and SAD, stabilized by intramolecular electrostatic interaction

and also could indicate a potential role of the phenolic hydroxyl group. The viability of this model is subject to experimental confirmation by potency of modified analogues designed to exploit features of NAD^+ binding.

Experimental Section

Mycophenolic acid was purchased from Sigma Chemical Co. and used without further purification. Ethanol was freshly distilled prior to use. All semiempirical calculations were performed with MPOAC 6.0 using the PM3 method with overall charge set to −1 for all NAD^+ and MPA models.

Preparation of the Na Salt of Mycophenolic Acid. A solution of mycophenolic acid in ethanol was treated with equimolar sodium ethylate at room temperature and stirred for 30 min. The solvent was evaporated in vacuo.

Nuclear Magnetic Resonance. ^{1}H-NMR spectra were recorded on a Varian VXR-400 multinuclear instrument. All spectra were measured using concentrations of 8.3 mg/cm^3 in D_2O with 2,2,3,3-tetradeuterio-3-(trimethylsilyl)propionic acid sodium salt (DSS) as internal standard (0.00 ppm). Homonuclear selective ^{1}H-[^{1}H] NOE data were obtained by the difference method[28] using frequency cycling techniques[29] for selective preirradiation. 2D ROESY spectra were collected using standard pulse programs. Other details were as follows: relaxation delay, $D_1 = 3$ s; mixing time, 1 s; sweep width, 4409 Hz in F_1 and F_2; 2048 data points in t_2; 256 experiments in t_1.

Molecular Modeling. All calculations and molecular modeling were performed by SYBYL 6.1 with an interface to MOPAC 6.0. All molecular dynamics simulations were carried out starting from the X-ray structure fully optimized by PM3 (precise criteria) applying the following setting: atomic charges were derived from PM3 Mulliken populations, nonbonded interactions were cut off at 8.0 Å and updated every 25 fs (every 1 fs in the aqueous simulation), and distance dependent dielectric constant and Tripos force field were used.

In the free MD calculation in vacuo the starting structure was heated to 700 K over 20 ps. Boltzmann distribution of initial velocities was used with a coupling factor of 100 fs. Following 30 ps equilibration period (T = 700 K, initial velocities; previous, coupling factor: 100 fs), the analysis was carried out over 100 ps at 700 K. The coupling constant 10 fs and previous velocities were used to collect one snapshot in every 100 fs to yield a total of 1000 conformations which were compared with the Family option of SYBYL upon the following torsional angles: C12−O11−C5−C6 (grid 60), C2′−C1′−C6−C7 (grid 40), C3′−C2′−C1−C6 (grid 40), and C5′−C4′−C3′−C2′ (grid 40). The representatives were fully optimized by Tripos force field followed by PM3 and analyzed.

The simulated annealing calculation in vacuo was repeated over 10 cycles using the built-in module of SYBYL. The following four experimental distances were introduced with a force constant of 15 kcal/mol Å^2: C(12)H$_3$−C(7′)H$_3$, C(12)H$_3$−C(1′)H$_2$, C(12)H$_3$−C(2′)H, and C(7′)H$_3$−C(1′)H$_2$. The starting structures were heated to 700 K over 2 ps and annealed to 200 K over 5 ps with an exponential annealing function. The final conformations were collected and energy minimized with molecular mechanics (Tripos force field). The obtained conformations were fully optimized without constrains with PM3 (precise criteria) and evaluated.

For the simulated annealing calculation in water, the constrained starting structure was solvated with 750 water molecules by SYBYL's Solvent/Lattice option. The system was equilibrated at 300 K for 2 ps with 0.5 fs time step and 10 fs coupling factor. Boltzmann distribution of initial velocities and periodic boundary conditions $x = y = z = 118.26$ Å were used. Then the time step was set to 1 fs, and the following intervals were assigned with previous initial velocities using the conditions described above: 1 ps at 700 K, 0.5 ps at 500 K, 0.75 ps at 350 K, and 1 ps at 200 K.

Conformational Analysis. The least-squares fit calculations were carried out by the corresponding module of SYBYL with equally weighed atom pairs. Dot surfaces were displayed at 1.1 x vdW atom radii with a density of 70/Å^2 and colored by electrostatic isopotentials (calculated from PM3 Mulliken populations by the point-charge method[17]) on the following scale (kcal/mol): red, > 24.9; orange, 24.9−9.96; yellow, 9.96−3.32; green, 3.32−0; cyan, 0−(−3.32); blue, (−3.32)−(−9.96); purple, (−9.96)−(−24.9); white, <−24.9.

Acknowledgment. This work was supported by Grant No. CA54507 from the National Cancer Institute.

References

(1) (a) Stet, E. H.; De Abreu, R. A.; Janssen, Y. P.; Bokkerink, J. P.; Trijbels, F. J. A Biochemical Basis for Synergism of 6-Mercaptopurine and Mycophenolic Acid in Molt F4, a Human Malignant T-Lymphoblastic Cell Line. *Biochim. Biophys. Acta* **1993**, *1180*, 277−282. (b) Stet, E. H.; Deabreu, R. A.; Bokkerink, J. P. M.; Lambody, L. H. J.; Vogelsmentink, T. M.; Trijbels, F. J. M. Inhibition of IMP Dehydrogenase by Mycophenolic Acid in Molt F4 Human Malignant Lymphoblasts. *Ann. Clin. Biochem.* **1994**, *31*, 174−180. (c) Wilson, B. S.; Deanin, G. G.; Standefer, J. C.; Vanderjagt, D.; Oliver, J. M. Depletion of Guanine Nucleotides with Mycophenolic Acid Suppresses Ige Receptor-Mediated Degranulation in Rat Basophilic Leukemia Cells. *J. Immunol.* **1989**, *143*, 259−265. (d) Mitsui, A.; Matsuno, T.; Ogawa, H.; Shiio, T.; Yugari, Y.; Tamura, G. Antitumor Activity of a New Compound, Ethyl O-[N-(P-Carboxyphenyl)-carbamoyl]-mycophenolate, Against Various Experimental Tumors Upon Oral Administration. *Gann* **1981**, *72*, 66−71. (e) Bates, T. A Preliminary Clinical Study of the Use of Mycophenolic Acid as a Radiosensitizer. *Eur. J. Cancer* **1977**, *13*, 475−477. (f) Suzuki, S.; Mori, T. Carbamoyl Mycophenlic Acid Ethylester, an Oral Antitumor Agent. *J. Antibiot.* **1976**, *29*, 286−291. (g) Suzuki, S.; Takaku, S.; Mori, T. Antitumor Activity of Derivatives of Mycophenolic Acid. *J. Antibiot.* **1976**, *29*, 275−285. (h) Connolly, J. G.; Halsall, G. M. Use of Mycophenolic Acid in Superficial Bladder Cancer. *Urology* **1975**, *5*, 131−132. (i) Knudtzon, S.; Nissen, N. I. Clinical Trial with Mycophenolic Acid (NSC-129185), a New Antitumor Agent. *Cancer Chemother. Rep. Part 1* **1972**, *56*, 221−227. (j) Sweeney, M. J.; Gerzon, K.; Harris, P. N.; Holmes, R. E.; Poore, G. A.; Williams, R. H. Experimental Antitumor Activity and Preclinical Toxicology of Mycophenolic Acid. *Cancer Res.* **1972**, *32*, 1795−1802. (k) Sweeney, M. J.; Hoffman, D. H.; Poore, G. A. Possible In Situ Activation of Mycophenolic Acid by Beta-Glucuronidase. *Cancer Res.* **1971**, *32*, 477−478. (l) Suzuki, S.; Kimura, T.; Ando, K.; Sawada, M.; Tamura, G. Antitumor Activity of Mycophenolic Acid. *J. Antibiot.* **1969**, *22*, 297−302.

(2) (a) Berman, J. D.; Webster, H. K. In Vitro Effects of Mycophenolic Acid and Allopurinol Against Leishmania Tropica in Human Macrophages. *Antimicrob. Agents Chemother.* **1982**, *21*, 877−891. (b) Verham, R.; Meek, T. D.; Hedstrom, L.; Wang, C. C. Purification, Characterization, and Kinetic Analysis of Inosine 5′-Monophosphate Dehydrogenase of Tritrichomonas Foetus. *Mol. Biochem. Parasitol.* **1987**, *24*, 1−12. (c) Noto, T.; Sawada, M.; Ando, K.; Koyama, K. Some Biological Properties of Mycophenolic Acid. *J. Antibiot.* **1969**, *22*, 165−169.

(3) (a) Alfieri, C.; Allison, A. C.; Kieff, E. Effect of Mycophenolic Acid on Epstein-Barr Virus Infection of Human B-Lymphocytes. *Antimicrob. Agents Chemother.* **1994**, *38*, 126−129. (b) Cline, J. C.; Nelson, J. D.; Gerzon, K.; Williams, R. H.; DeLong, D. C. In Vitro Antiviral Activity of Mycophenolic Acid and Its Reversal by Guanine-Type Compounds. *Appl. Microbiol.* **1969**, *18*, 14−20. (c) Planterose, D. N. Antiviral and Cytotoxic Effects of Mycophenolic Acid. *J. Gen. Virol.* **1969**, *4*, 629−630. (d) Williams, R. H.; Lively, D. H.; DeLong, D. C.; Cline, J. C.; Sweeney, M. J. Mycophenolic Acid: Antiviral and Antitumor Properties. *J. Antibiot.* **1968**, *21*, 463−464.

(4) (a) Gomez, E. C.; Menendez, L.; Frost, P. Efficacy of Mycophenolic Acid for the Treatment of Psoriasis. *J. Am. Acad. Dermatol.* **1979**, *1*, 531−537. (b) Sweeney, M. J. Mycophenolic Acid and Its Mechanism of Action in Cancer and Psoriasis. *J. Antibiot.* **1977**, *30S*, 85−92. (c) Marinari, R. Fleischmajer, R.; Schragger, A. H.; Rosenthal, A. L. Mycophenolic Acid in the Treatment of Psoriasis: Long-Term Administration. *Arch. Dermatol.* **1977**, *113*, 930−932. (d) Lynch, W. S.; Roenigk, H. H., Jr. Mycophenolic Acid for Psoriasis. *Arch. Dermatol.* **1977**, *113*, 1203−1208.

(5) (a) Yamada, Y.; Natsumeda, Y.; Weber, G. Action of the Active Metabolites of Tiazofurin and Ribavirin on Purified IMP Dehydrogenase. *Biochemistry* **1988**, *27*, 2193−2196. (b) Lee, H.-J.; Pawlak, K.; Nguyen, B. T.; Robins, R. K.; Sadee, W. Biochemical Differences Among Four Inosinate Dehydrogenase Inhibitors, Mycophenolic Acid, Ribavirin, Tiazofurin, and Selenazofurin, Studied in Mouse Lymphoma Cell Culture. *Cancer Res.* **1985**, *45*, 5512−5520. (c) Gebeyehu, G.; Marquez, V. E.; Van Cott, A.; Cooney, D. A.; Kelley, J. A.; Jayaram, H. N.; Ahluwalia, G. S.; Dion, R. L.; Wilson, Y. A.; Johns, D. G. Ribavirin, Tiazofurin, and Selenazofurin: Mononucleotides and Nicotinamide Adenine Dinucleotide Analogues. Synthesis, Structure, and Interactions with IMP Dehydrogenase. *J. Med. Chem.* **1985**, *28*, 99−105.

(6) Hedstrom, L.; Wang, C. C. Mycophenolic Acid and Thiazole Adenine Dinucleotide Inhibition of *Tritrichomonas foetus* Inosine Monophosphate Dehydrogenase: Implications on Enzyme Binding. *Biochemistry* **1990**, *29*, 849−854.
(7) (a) Goldstein, B. M.; Bell, J. E.; Marquez, V. E. Dehydrogenase Binding by Tiazofurin Anabolites. *J. Med. Chem.* **1990**, *33*, 1123−1127. (b) Li, H.; Hallows, W. H.; Punzi, J. S.; Marquez, V. E.; Carell, H. L.; Pankiewicz, K. W.; Watanabe, K. A.; Goldstein, B. M. Crystallographic Studies of Two Alcohol Dehydrogenase-Bound Analogues of Thiazole-4-carboxamide Adenine Dinucleotide (TAD), the Active Anabolite of the Antitumor Agent Tiazofurin. *Biochemistry* **1994**, *33*, 23−32.
(8) SYBYL 6.1, Tripos Associates Inc.; MOPAC 6.0 (QCPE #455).
(9) SYBYL's Multifit command.
(10) Wu, Y.-D.; Houk, K. N. Theoretical Study of Conformational Features of NAD^+ and NADH Analogs: Protonated Nicotinamide and 1,4-Dihydronicotinamide. *J. Org. Chem.* **1993**, *58*, 2043−2045.
(11) Protein Data Bank, Chemistry Department, Brookhaven National Laboratory, Upton, NY 11973.
(12) (a) Oppenheimer, N. J.; Marschner, T. M.; Malver, O.; Kam, B. L. Stereochemical Aspects of Coenzyme-Dehydrogenase Interactions. In *Mechanism of Enzymatic Reactions: STEREOCHEMISTRY*; Frey, P. A., Ed.; Elsevier Science Publishing Co.: New York, 1986; pp 15−28. (b) Benner, S. A.; Nambiar, K. P. Functional Explanations for Stereoselectivity in Dehydrogenases. In *Mechanism of Enzymatic Reactions: STEREOCHEMISTRY*; Frey, P. A., Ed.; Elsevier Science Publishing Co.: New York, 1986; pp 29−43.
(13) Jayaram, H. N.; Johns, D. G. Metabolic and Mechanistic Studies with Tiazofurin (2-b-D-ribofuranosylthiazole-4-carboxamide). In *Developments in Cancer Chemotherapy*; Glazer, R. I., Ed.; CRC Press: Boca Raton, FL, 1984; pp 115−130.
(14) Burling, F. T.; Goldstein, B. M. Computational Studies of Nonbonded Sulfur-Oxygen and Selenium-Oxygen Interactions in the Thiazole and Selenazole Nucleosides. *J. Am. Chem. Soc.* **1992**, *114*, 2313−2320.
(15) Brookhaven data bank file 1grb.full.
(16) Eklund, H.; Samama, J.-P.; Jones, T. A. Crystallographic Investigation of Nicotinamide Adenine Dinucleotide Binding to Horse Liver Alcohol Dehydrogenase. *Biochemistry* **1984**, *23*, 5982−5996.
(17) Cox, S. R.; Williams, D. E. Representation of the Molecular Electrostatic Potential by a Net Atomic Charge Model. *J. Comput. Chem.* **1981**, *2*, 304−323.
(18) Walters, D. E.; Hinds, R. M. Genetically Evolved Receptor Models: A Computational Approach to Construction of Receptor Models. *J. Med. Chem.* **1994**, *37*, 2527−2536.
(19) Root mean square value: rms = $(\sum d^2/n)^{1/2}$.
(20) Anderson, W. K.; Boehm, T. L.; Makara, G.; Swann, R. T. Synthesis and Modeling Studies with Monocyclic Analogues of Mycophenolic Acid. *J. Med. Chem.* **1996**, *39*, 46−55.
(21) Jones, D. F.; Mills, S. D. Preparation and Antitumor Properties of Analogs and Derivatives of Mycophenolic Acid. *J. Med. Chem.* **1971**, *14*, 305−311.
(22) Cram, D. J. The Design of Molecular Hosts, Guests, and Their Complexes. *Science* **1988**, *240*, 760−767.
(23) Goldstein, B. M.; Li, H.; Hallows, W. H.; Langs, D. A.; Franchetti, P.; Cappellacci, L.; Grifantini, M. C-glycosyl Bond Conformation of Oxazofurin-Crystallographic and Computational Studies of the Oxazole Analogue of Tiaofurin. *J. Med. Chem.* **1994**, *37*, 1684−1688.
(24) Hupe, D. J.; Azzolina, B. A.; Behrens, N. D. IMP Dehydrogenase from the Intracellular Parasitic Protozoan Eimeria Tenella and Its Inhibition by Mycophenolic Acid. *J. Biol. Chem.* **1986**, *261*, 8363−8369.
(25) Jackson, R. C.; Weber, G.; Morris, H. P. IMP Dehydrogenase, an Enzyme Linked with Proliferation and Malignancy. *Nature* **1975**, *256*, 331−333.
(26) Baker, P. J.; Britton, K. L.; Engel, P. C.; Farrants, G. W.; Lilley, K. S.; Rice, D. W.; Stillman, T. J. Subunit Assembly and Active Site Location in the Structure of Glutamate Dehydrogenase. *Proteins* **1992**, *12*, 75−86.
(27) Harrison, W.; Shearer, M. M.; Trotter, J. Crystal Structure of Mycophenolic Acid. *J. Chem. Soc., Perkin Trans. II* **1972**, 1542−1544.
(28) Sanders, J. K. M.; Mersh, J. D. Nuclear Magnetic Double Resonance: the Use of Difference Spectroscopy. *Prog. Nucl. Magn. Reson. Spectros.* **1983**, *15*, 353−400.
(29) Kinns, M.; Sanders, J. K. M. Improved Frequency Selectivity in Nuclear Overhauser Effect. *J. Magn. Reson.* **1984**, *56*, 518−520.

JM950600M